THE ASTROPHYSICAL JOURNAL, 428:363–369, 1994 June 10

NEAR-INFRARED SPECTROMETER ON THE INFRARED TELESCOPE IN SPACE

MANABU NODA,[1] TOSHIO MATSUMOTO, SHUJI MATSUURA, KUNIO NOGUCHI,
MASAHIRO TANAKA, AND MARK A. LIM[2]
Department of Astrophysics, School of Science, Nagoya University, Chikusa-ku, Nagoya 464-01, Japan
AND
HIROSHI MURAKAMI
Institute of Space and Astronautical Science, Sagamihara, Kanagawa 229, Japan
Received 1993 February 2; accepted 1993 December 10

ABSTRACT

The Near-Infrared Spectrometer (NIRS) is a grating spectrometer with two 12 element InSb linear arrays, and is one of the four focal-plane instruments of the Infrared Telescope in Space (IRTS) mission, which will be launched in early 1995. The NIRS was designed to measure the absolute sky brightness with coarse spectral resolution; searching for extragalactic background light is the primary purpose of our observations. The wavelength coverage of the NIRS ranges from 1.4 to 4.0 μm with a spectral resolution of 0.12 μm. The field of view is $8' \times 8'$. The NIRS has been calibrated and tested with the flight IRTS telescope in the laboratory. The response and noise were found to be as expected from the design values. After integrating all of the focal-plane instruments with the telescope into the flight cryostat, NIRS shows good performance and will be able to achieve a high sensitivity in orbit.

Subject headings: artificial satellites, space probes — infrared: general — instrumentation: spectrographs

1. INTRODUCTION

The Infrared Telescope in Space (IRTS) is a cooled telescope that is scheduled to be launched on the first *Space Flyer Unit* mission (*SFU-1*) from Tanegashima Space Center in early 1995. The *SFU* is a multipurpose satellite on which many experiments are loaded, and will be placed in a nearly circular, 482 km altitude, 28°.5 inclination orbit (Natori & Kuriki 1991). During about 3 weeks of observing, the *SFU* mission will be dedicated to IRTS observations. After a period of 6–18 months from launch, the *SFU-1* is scheduled to be retrieved by NASA's Space Transportation System for refurbishment and reuse in the future.

The IRTS will orbit the Earth with the telescope sweeping across the sky at a rate of $4' \ s^{-1}$ in great circles (Murakami et al. 1994). The axis of the great circle will be fundamentally pointed to the Sun and precessed at a rate of approximately $4'$ orbit^{-1}. Approximately 10% of the sky will be observed in the anticipated 3 week mission.

The IRTS telescope is of Ritchey-Chrétien design with gold-coated aluminum optics (Onaka et al. 1994). The system of baffles employs a combination of sunshade, passively cooled aperture shade, cryogenically cooled specular forebaffle, and black aftbaffle (Sato et al. 1994). The telescope size of the IRTS is small (15 cm diameter), but the IRTS is optimized to observe diffuse extended infrared sources. Four scientific instruments and a star sensor (germanium photovoltaic detector) share a common focal plane in the IRTS telescope. This paper describes one of the instruments, the Near-Infrared Spectrometer (NIRS). Descriptions of the other three instruments (Mid-Infrared Spectrometer [MIRS], Far-Infrared Line Mapper [FILM], and Far-Infrared Photometer [FIRP]) and the telescope facility can be found in other references (Roellig et al. 1994; Shibai et al. 1994; Lange et al. 1994; Murakami et al. 1994; Onaka et al. 1994; Sato et al. 1994).

The NIRS is a simple grating spectrometer covering wavelengths from 1.4 to 4.0 μm, with a resolution of 0.12 μm. The field of view is $8' \times 8'$. The NIRS was designed to measure the absolute sky brightness with coarse spectral resolution. The origin of the light of the night sky has been one of the interesting subjects of astrophysics. The diffuse near-infrared background mainly consists of zodiacal light, thermal emission from interplanetary dust, starlight, and extragalactic background light (EBL). The spectral information obtained by the NIRS is useful to separate the light into these components. The NIRS was optimized for diffuse sources, but it can also observe bright point sources because the field of view is relatively small.

The NIRS observations are unique as compared with other previous and future observations. The *Infrared Astronomical Satellite* (*IRAS*; Neugebauer et al. 1984) showed the great advantage of the orbiting cooled infrared telescope and contributed to revealing the general infrared view of the universe. There were, however, only four photometers centered at 12, 25, 60, and 100 μm, and a low spectral resolution spectrometer operating from 8 to 23 μm.

The Diffuse Infrared Background Experiment (DIRBE) on the *Cosmic Background Explorer* (*COBE*) satellite, which was launched in 1989, was designed to conduct a sensitive search for an isotropic cosmic infrared background (Hauser et al. 1991). It observed the entire sky with a $0°.7 \times 0°.7$ field of view in 10 different bands from 1.2 to 240 μm, including the standard *J*, *K*, *L*, and *M* bands (Hauser 1993). It also observed the polarization of the sky at the *J*, *K*, and *L* bands (Berriman et al. 1993). Compared with DIRBE, the NIRS is characterized by spectral observations with smaller beam size.

The *Infrared Space Observatory* (*ISO*), which will be launched in 1995, plans to measure the extragalactic background from the near-infrared to the far-infrared by photom-

[1] Present address: Nagoya Municipal Industrial Research Institute.
[2] Present address: Physics Department, University of California at Santa Barbara.

etry or imaging in selected areas. ISO has a coarse resolution grating spectrometer from 2.5 to 12 μm (ISOPHOT-S), but the sensitivity for diffuse sources is worse than that of the NIRS. A nonbiased survey with high sensitive spectrometry characterizes the NIRS in comparison with *ISO*.

2. ASTROPHYSICAL OBJECTS

2.1. *Zodiacal Light*

The zodiacal light, which is sunlight scattered by interplanetary dust (IPD), has been studied in the ultraviolet and the optical band. An all-sky map of the zodiacal light at the V band (0.50 μm) was summarized by Levasseur-Regourd & Dumont (1980). The color of the zodiacal light has been found to be close to the solar color (Leinert 1975). Based on these observations, various models for the volume scattering function and space distribution of the IPD have been proposed (Lamy & Perrin 1986). In the near-infrared region, there have been few observations of the zodiacal light. If the size of the dust grains is comparable to the wavelength of visible light, the color of the zodiacal light in the near-infrared would have to be bluer than the solar color. Matsumoto, Akiba, & Murakami (1988, hereafter MAM) reported that the color of the zodiacal light is bluer than the solar spectrum, but a recent rocket observation (Noda et al. 1992) indicates that near-infrared color of the zodiacal light is close to the solar color. Information on the near-infrared spectrum with wide sky coverage will reveal the size and spatial distribution of the dust.

At longer wavelengths, *IRAS* observed the thermal emission of the IPD with almost complete sky coverage (Hauser et al. 1984). From *IRAS* observations, the temperature of the IPD was estimated to be 275 ± 57 K (graybody) at the ecliptic pole and 244 ± 44 K (graybody) at the ecliptic plane, but MAM suggested that the temperature of the IPD is about 205 K (graybody). The DIRBE on *COBE* has obtained photometric maps of the full sky from 1.2 to 240 μm (Hauser 1993). Detailed analysis will add new information about IPD. The NIRS on the IRTS, together with the MIRS (from 4.5 to 11.7 μm), will give us an almost continuous spectrum of the Wien part of the thermal emission of the IPD. The spectrum data will be important to estimate the temperature of the IPD and investigate the composition of the interplanetary dust particles.

2.2. *Diffuse Galactic Light*

The main component of starlight in the near-infrared is emission from faint late-type stars. A near-infrared balloon-borne survey of the Galactic plane clearly revealed the stellar distribution (Hayakawa et al. 1981) but was performed only for the Galactic plane with a few infrared wavelength bands, which do not suffer strong atmospheric emission. The spectral coverage and resolution of the NIRS will allow observation of molecular bands (e.g., CO at 4.6 μm, H_2O at 2.7 μm) from late-type stars. Observations of stars at high Galactic latitude are important in studying the nature of the Galactic halo stars.

Unidentified infrared bands (3.3, 3.4, 6.2, 7.7, 8.6, 11.3 μm, etc.) have been observed in planetary nebulae (Gillett, Forrest, & Merrill 1973; Russell, Soifer, & Willner 1977). The origin of these IR emission features is suggested to be polycyclic aromatic hydrocarbons (PAHs) heated by absorption of single UV photons of the interstellar radiation field (Léger & Puget 1984). A 3.3 μm feature in the diffuse emission of the Galactic disk was reported by Giard et al. (1988). The NIRS and the MIRS will be able to observe these spectral features in various sites: circumstellar clouds, star-forming regions, and general interstellar clouds. Not only the intensities of these band emissions but also correlation with the [C II] line emission and the far-infrared dust emissions observed by the FILM and the FIRP will give us information about the composition of the interstellar dust and the physical conditions of the interstellar radiation field.

2.3. *Extragalactic Background Light*

Although it has not been observed unambiguously so far, an infrared extragalactic background has been postulated to exist in cosmological theories (Partridge & Peebles 1967). The infrared extragalactic background light (EBL) is the integration of redshifted light from galaxies or Population III stars, which would have emitted a huge amount of UV and optical radiation (Carr, Bond, & Arnett 1984; McDowell 1986). A spectral window exists in foreground emission in the vicinity of 3 μm (cf. Fig. 8), in which the infrared EBL may be observable.

Since the 1970s, searches for the EBL have been tried in the optical and near-infrared region, but have produced only upper limits because of strong foreground emissions or thermal emission from the instruments (Hofmann & Lemke 1978; Mattila 1990). Recently, the brightness of the EBL has been derived from galaxy counts (Tyson 1990; Cowie et al. 1990). Near-infrared observations using sounding rockets with cooled optics have attempted to measure the EBL (MAM; Noda et al. 1992). These rocket observations suggested unknown isotropic emission $\sim 10^{-11}$ W cm^{-2} sr^{-1} in the K band, which would be attributed to an extragalactic origin. The DIRBE result shows almost the same absolute sky brightness with the rocket observations, but the shape of the energy distribution is reported to be different and some doubt about the rocket measurements is indicated (Hauser et al. 1991). In order to discriminate the EBL from the observed sky brightness, careful analysis and modeling of the DIRBE data will be expected. The NIRS spectral observation which covers the "window" in the near-infrared will give us more reliable information about the EBL.

2.4. *Point Sources*

Because of its moderate spatial resolution and high sensitivity the NIRS will be able to separate stars brighter than 7th K magnitude from the diffuse background and measure their near-infrared spectrum. Combining the NIRS data with the data from the MIRS will produce continuum spectra from 1.4 to 11.7 μm, the wavelength region containing H_2O, H_2O ice, CO, Si, and SiC bands. The NIRS and MIRS observations will measure spectra of sources at shorter wavelength and one or two orders of magnitude fainter than the low-resolution spectrometer of *IRAS*. These data will be valuable for studying evolution and physical process of late-type stars.

3. INSTRUMENT

The NIRS is a grating spectrometer with two 12 element InSb (indium antimonide) linear arrays. In order to achieve a good signal-to-noise ratio (S/N), we have developed a sensitive and low-noise detection system, with an InSb detector array and a charge integrating amplifier. Given the performance of the detector system, we fixed the field of view to be $8' \times 8'$ and the spectral resolution to be $\Delta\lambda = 0.12$ μm. The characteristics of the NIRS are summarized in Table 1.

TABLE 1

CHARACTERISTICS OF NIRS

Characteristic	Value or Specification
Size (mm^3)	135 × 154 × 102 overall
Weight (kg)	1.18
Entrance aperture (mm^2)	1.4 × 1.4
Field of view ($arcmin^2$)	8 × 8
Temperature (K)	~1.8
Detection system:[a]	
Detector	InSb
Element size (mm^2)	1 × 0.5 (per element)
Number of elements	24 (2 × 12 elements)
Wavelength coverage (μm)	1.43–2.54, 2.88–3.98[b]
Resolution (μm)	0.12 (0.10 at channel 1)
Dark current (A)	Several times 10^{-17}
Total capacitance (pF)	~50
Readout method	Charge-integrating amplifier
Temperature of J-FETs (K)	~70

[a] Two 12 channel linear arrays with low-resolution grating spectrometer.
[b] 0.1 μm interval.

3.1. *Spectrometer*

The schematic view of the optical system of the NIRS is shown in Figure 1. The 1.4 mm × 1.4 mm slit is located at the IRTS telescope focal plane. The cylindrical mirrors (CM1 and CM2) change the f/4 beam to f/8 along the Z-axis only. A large f-number makes the spectrometer compact with small aberrations. The beam is made parallel by the parabolic mirror (PM) and is diffracted by the grating. It is focused again on the detector by the spherical mirror (SM). The two 12 element InSb linear arrays are aligned in the focal sphere, and each of them has an order-sorting bandpass filter. The wavelength range of the shorter wavelength array is from 1.43 to 2.54 μm, and that of the longer wavelength side is from 2.88 to 3.98 μm. A channel number is assigned to each detector element in order of increasing wavelength.

The grating of the NIRS, made by Hitachi Corporation, has a ruling number of 93 lines mm^{-1}, a blaze angle of 4°.8, and a blaze wavelength of 1.80 μm. The aluminum mirrors were machined and polished by Nikon Corporation. Their surface is coated with Au and SiO_2, and has a measured reflectivity of more than 96% from 1 to 5 μm.

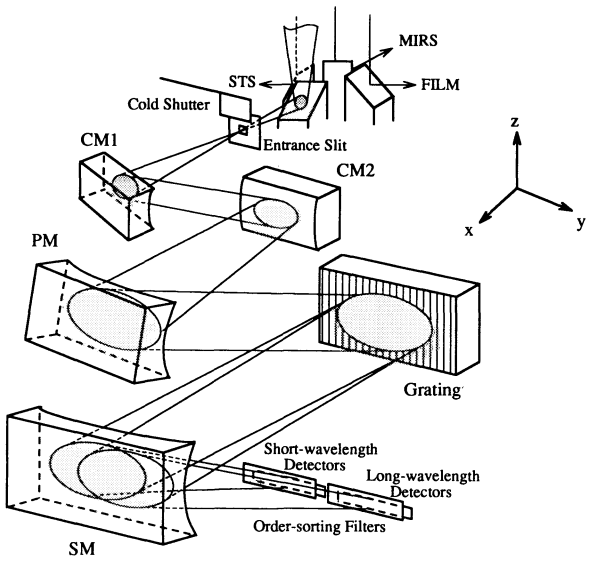

FIG. 1.—Schematic view of the optical system of the near-infrared spectrometer.

In order to calibrate DC drifts of the electronics and to measure the zero signal level, a cold shutter is located at the entrance slit and is closed for 8 s every 66 s automatically. A small tungsten lamp is installed near the shutter for an internal calibrator, which turns on for 8 s every 17.5 minutes to monitor the stability and linearity of the instrumental response.

3.2. *Detection System*

Each channel of the detection system consists of an InSb photodiode and a charge-integrating amplifier. The InSb array detector was developed under a collaboration with Hamamatsu Photonics K.K. (Murakami et al. 1987; Yamamoto et al. 1989). Important features of this detector are its low capacitance and very low dark current at low temperature. Since a large capacitance increases the voltage noise of the amplifier, the low capacitance of the detector reduces the system noise. For the flight detector module, the element size is 1 mm × 0.5 mm, and the total capacitance, including stray capacitance, is about 50 pF. The typical dark current at 2 K is several times 10^{-17} A.

The charge-integrating amplifier, consisting of an InSb photodiode and three field effect transistors (FETs), shows better noise performance than the usual TIA at longer integration time (Murakami et al. 1988; Yamamoto et al. 1989; Noda 1991). Figure 2 shows a portion of the circuit diagram of the 24 channel array. Charges generated by incident photons are integrated in the electric capacitance of the photodiode and are read out nondestructively without transfer. The integrated charges are periodically discharged every 66 s through a reset FET. The detectors are not explicitly biased in this system. They are automatically biased to about 100 mV by a charge injection following a charge reset. The well capacity is typically 3×10^7 electrons. The dynamic range required for the NIRS observation is about 10% of the total capacity, which guarantees a good linearity. The corresponding values of noise equivalent power are 2×10^{-17} W at 1 s integration, and $\leq 3 \times 10^{-18}$ W for longer than 10 s integration. The linear improvement of S/N with integration time is the important feature of the charge-integrating amplifier.

The operating temperature of the InSb detectors is 1.8 K, but the J-FETs do not work well below 50 K. Thus, the J-FETs have to be thermally isolated from the cryogenic work surface, and their temperature must be controlled to about 70 K.

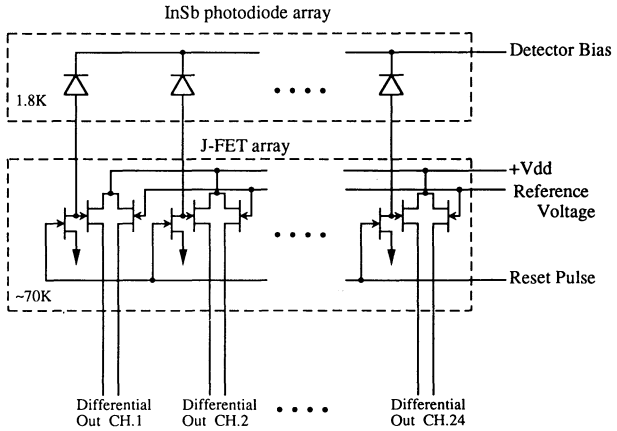

FIG. 2.—Portion of the circuit diagram of the 24 channel array

Twenty-four discrete sets of amplifiers are mounted on a thin sapphire substrate, which has both good electrical isolation and high thermal conductivity at low temperature. On the substrate, a metal film resistor and a platinum chip resistor are also installed and a bridge circuit was used to keep the resistance of platinum constant. This circuit can control temperatures around 70 K with 50 mK stability, and the settling time from turn-on is about 5 minutes.

The sapphire substrate is suspended from the frame by bundles of aramid fibers, and 10 μm stainless wires are used for signal lines from the sapphire substrate to the frame. This design has low thermal conductivity and is strong enough to survive the vibrations at the launch of the satellite. A few milliwatts is necessary to keep the temperature of J-FETs around 70 K, given the thermal conductivity of the aramid fibers.

3.3. *Warm Electronics and Telemetry Data*

A block diagram of the warm electronics, constructed by Hamamatsu Photonics K.K., is shown in Figure 3. The output signals from the cold electronics are coupled to discrete low-noise differential amplifiers. Since the mismatch of the dual J-FETs results in scattered output signals, individual offset amplifiers are used after the preamplifiers in order to cancel this scatter. The total gain of the warm electronics is 1600, and the sampling frequency for each detector is 4 Hz.

Data from all four of the focal-plane instruments, a star sensor, and telescope housekeeping are multiplexed into a 6 kbytes s^{-1} common telemetry stream, and stored in the spacecraft's 80 Mbit bubble memory. The data are telemetered to the ground during brief downlinks as the spacecraft passes over receiving stations in NASA's Deep Space Network and Japan's Kagoshima Space Center. After recording and one-site archiving, the data will be transmitted to the IRTS Sagamihara Operating Center at the Institute for Space and Astronautical Science (ISAS) for processing. The entire IRTS data set will eventually be made available to the public through the Image Processing and Analysis Center (IPAC) in the United States.

4. CALIBRATION IN THE LABORATORY

4.1. *Individual Spectroscopy*

Initially, the optical system was aligned using a He-Ne laser at room temperature. The higher orders of laser light were aligned onto the corresponding positions of the detector array. The order-sorting filters were removed during this alignment. Next, the NIRS was installed on the cold plate of a 12 inch (30 cm) Dewar and was cooled to 4.2 K by liquid helium. The spectral response was measured using a calibrated monochrometer at Nagoya University. The measurements were carried out with a CaF_2 vacuum window. A cold fused quartz window at the outer radiation shield ($\sim$100 K) which blocked long-wavelength radiation was used to achieve a low thermal background condition. Since water was excluded from this fused quartz, there were no absorption bands of H_2O at 2.7 μm. A CaF_2 lens, placed between monochrometer and the NIRS, made a f/4 beam corresponding to the f-number of the IRTS telescope. We ran air conditioners in order to keep the humidity low and purged the light path with dry N_2 gas, because some channels suffered absorption from molecules such as H_2O and CO_2.

The measured center wavelengths for the detectors ranged from 1.43 to 2.54 μm and from 2.88 to 3.98 μm, with a 0.10 μm interval. Spectral resolution (FWHM) was 0.12 μm except for channel 1. The short-wavelength end of channel 1 was defined by an order-sorting filter, which provided a bandwidth of 0.10 μm. The optical blocking properties of the spectrometer were

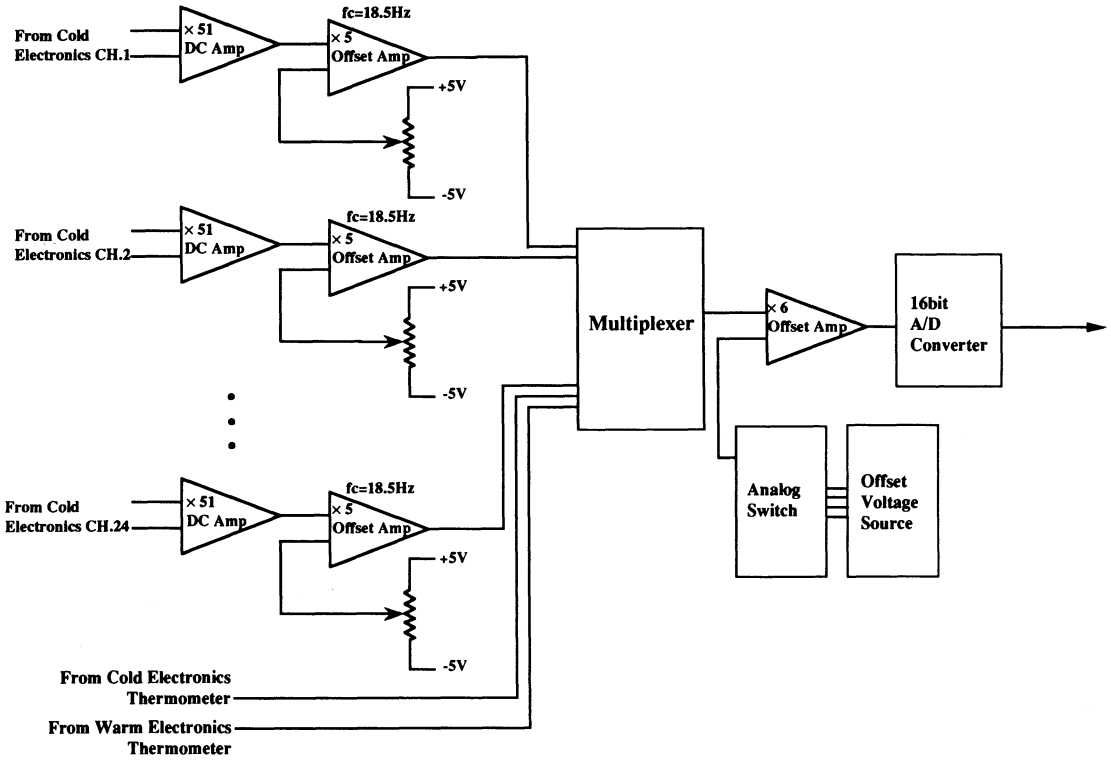

FIG. 3.—Block diagram of the NIRS warm electronics

verified below 10^{-3} for incident radiation from 1 to 5 μm, where InSb is sensitive.

4.2. *Absolute Calibration Using a Large-Size Blackbody*

The NIRS was mounted at the focal plane of the IRTS flight telescope at the ISAS. They were installed in a special test cryostat, and the absolute sensitivity to diffuse emission was measured. The absence of stray light or internal thermal background was verified by putting a cold lid in front of the telescope.

A CaF_2 vacuum window and a cold fused quartz window were also used for absolute calibration. The size of both windows was 170 mm, which was large enough not to interrupt the étendue of the NIRS. Since the $\sim$300 K emission from the laboratory was too strong for the longer wavelength channels, an aluminum plate with 1 mm diameter holes on a 10 mm $\times$ 10 mm grid was placed at the inner radiation shield. It reduced the incident light by 8.6×10^{-3}. The configuration of the calibration is schematically shown in Figure 4.

A large-aperture blackbody (180 mm diameter) was placed in front of the test cryostat, and output signals were measured for various temperatures of the blackbody. The temperature of the large-aperture blackbody could be varied from 312.6 K (39.4°C) to 469.6 K (196.4°C). An accurate measurement of the temperature is very important because our wavelength region belongs to the Wien part of the blackbody radiation curve. The sensitivity of the NIRS taken by these measurements is shown in Figure 5. The sensitivity is defined as

$$\frac{\Delta V(T)/\Delta t}{F_\lambda(T)\lambda_c/\Delta\lambda}\ \mathrm{V\ s^{-1}\ (W\ cm^{-2}\ sr^{-1})^{-1}}, \qquad (1)$$

where λ_c is the central wavelength of the channel, $\Delta\lambda$ is the spectral resolution, $\Delta V(T)$ is the increment of the output voltage for Δt(s), and $F_\lambda(T)$ is the incident flux calculated by the convolution of the blackbody spectrum at T(K) and the measured spectral response of each channel. This sensitivity gives the output response of the NIRS per unit surface brightness.

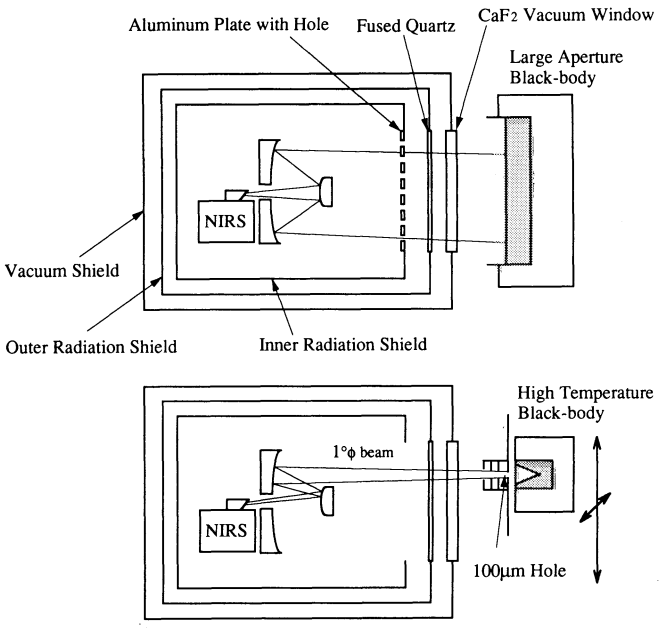

FIG. 4.—Schematic diagram of the absolute calibration

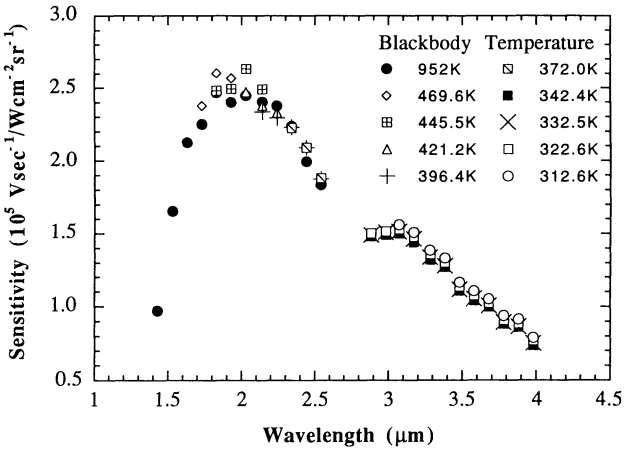

FIG. 5.—Sensitivity of the NIRS measured by different blackbody temperatures.

4.3. *Absolute Calibration Using a High-Temperature Blackbody*

For the short-wavelength channels, the input energy from the large-aperture blackbody was too small for an accurate calibration, so a high-temperature calibration source was necessary. We used a small, high-temperature blackbody (952 K) and measured the response as the blackbody was moved over a grid with 5 mm $\times$ 5 mm spacing. Since the aluminum plate with small holes on the inner radiation shield was removed for this measurement, the longer wavelength channels were saturated by the strong thermal background radiation from the laboratory. The middle-wavelength channels could confirm the consistency of the small-blackbody measurements with the large-blackbody measurements. We used a mask with a 100 μm hole and a baffle to make a 1° diameter beam which filled the solid angle of the NIRS beam. We also measured the signal of the room temperature's radiation and corrected the incident energy from the high-temperature blackbody.

The integrated value of the data after correction of the aperture size of the blackbody represents the output signal when the whole field of view of the NIRS is covered with the high-temperature blackbody. The calculated sensitivity defined in the previous section is shown in Figure 5 as filled circles. In spite of the extensive temperature change and the different methods, the discrepancy between the two methods is less than 5% at the overlapped wavelengths.

Based on the data from these experiments, the optical efficiency of the NIRS (including telescope) was estimated and is shown in Figure 6. For this estimate, we assumed that the field of view of the NIRS is a 8′ $\times$ 8′ rectangle, that the effective area of the telescope is 113 cm^2 (64% of the primary mirror), and that the quantum efficiency of the InSb is 0.5. The wavelength dependence of the estimated efficiency is mainly due to the characteristics of the grating. This optical efficiency was found to be as expected from the design value.

4.4. *Measurements with Collimated Beam*

The instrumental polarization, spectral response, and beam pattern of the NIRS were measured with a collimated beam. The test cryostat was aligned with a large (60 cm diameter) collimator mirror. A blackbody source was mounted on the X-Y stage at the focus of the collimator mirror, so that the image of the blackbody aperture was focused in the plane of the NIRS entrance slit.

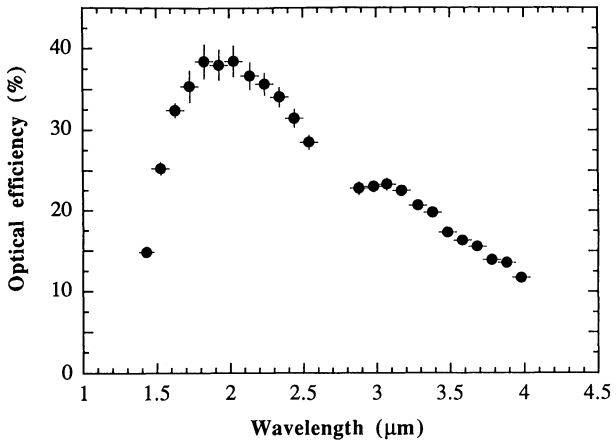

FIG. 6.—Optical efficiency of the NIRS

When we inserted a polarizer into the beam just in front of the blackbody, a significant instrumental polarization was observed. The position angle and the magnitude of polarization are shown in Figure 7. The position angle is defined from the direction parallel to the ruling direction. The magnitude of polarization is smallest and the position angle changes most rapidly in the vicinity of the blaze wavelength of the grating. This is due to the characteristics of the grating. In the wavelength range shorter than the blaze wavelength, the linearly polarized light along the direction parallel to the ruling direction is stronger than that along the perpendicular to it. In the longer wavelength region, the perpendicularly polarized light is stronger, and the magnitude of the polarization increases with increasing wavelength. The measured position angles in the longer wavelength region were not 90°, probably because of other polarization effects and the systematic error of the measurement of the angle. This instrumental polarization will add to the flux measurement uncertainties, because there is no a priori knowledge of the magnitude and direction of the polarization for the NIRS astronomical sources.

In place of the polarizer, a calibrated circular variable filter was inserted in front of the blackbody to confirm the spectral response of each detector. The result was consistent with the previous measurements using the calibrated monochrometer at Nagoya University.

Finally, we tried to measure the beam pattern of the NIRS by moving the blackbody on the *X-Y* stage. Because of the severe time limitation of the IRTS project, the measurement was made along a few paths parallel to the axis of the stage. The result only confirms that there is no serious problem in the optics of the NIRS. We plan to measure the beam pattern of the NIRS in orbit by using stars, and calibrate the sensitivity for a point source by using known standard stars.

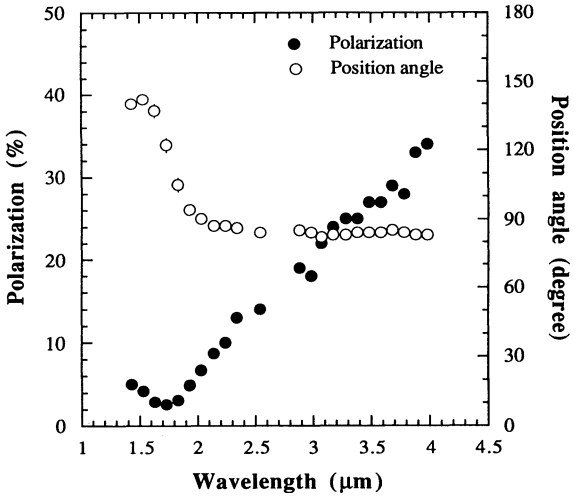

FIG. 7.—Measured polarization of the NIRS. Open circles represent the angle of polarization, and filled circles show the magnitude of polarization.

5. PERFORMANCE OF THE NIRS IN THE FLIGHT CRYOSTAT

After the calibration for each focal-plane instrument, optical and electromagnetic interference were measured for all scientific instruments and the star sensor using the test cryostat. The results were reflected to the construction of the electrical ground network, the optical shielding, and the timing of the calibration light for each instrument in the flight configuration.

All aligned components were carefully taken out of the test cryostat and reinstalled in the flight cryostat. Because of the release mechanism of the flight lid, a dark condition for all instruments cannot be realized in the flight configuration. A cold lid was placed in front of the telescope, and the absence of stray light or internal thermal background for all instruments was ascertained. After this test, we operated the IRTS system at the flight condition, and could confirm the basic performance of IRTS. The NIRS showed good noise performance in the flight cryostat and did not suffer interference from other instruments. During the tests which simulate the space environments, such as vibration and radio-frequency interference, no serious problems were observed in the NIRS performance. The rms noises of all the NIRS detectors were at normal levels of about 150 electrons for a several second integration time.

6. EXPECTED DETECTION LIMIT

The sensitivity of the NIRS, according to the calibrations and the noise performance, are shown in Figure 8. Open circles indicate the 1 σ sensitivity for 1 field of view (1 FOV) of the

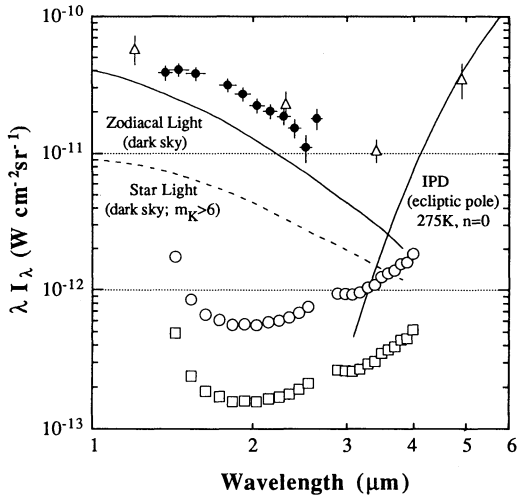

FIG. 8.—Detection limits of the NIRS. The total predicted sensitivity of the NIRS is shown by open circles (1 FOV, 1 σ) and by open squares (10 s integration, 1 σ). The observed sky brightness is also shown by filled circles and open triangles. Lines represent the estimated zodiacal light, starlight fainter 6th *K* magnitude at dark sky (higher ecliptic and Galactic latitude), and thermal emission of the IPD at the ecliptic pole.

NIRS. Since 1 FOV of the NIRS is 8′ × 8′ and the IRTS scans 4′ s^{-1} overlapping one-half of the 1 FOV, the sensitivity is calculated from the results of twice measured 2 s integration. At high Galactic latitudes there will be some areas where the NIRS observes no bright stars for more than 10 s. Open squares indicate the 1 σ detection limit for 10 s integration in such dark sky areas. Since the integrated charges are read out nondestructively at 4 Hz and reset automatically every 66 s, integration time can be taken up to 66 s. In this case, however, the space resolution becomes worse and the probability of source confusion becomes larger with increased integration time because of the scanning observation.

The sky brightness observed by recent rocket observation (Noda et al. 1992) and by *COBE* (Hauser et al. 1991) are also shown by filled circles and open triangles, respectively. Lines represent the estimated zodiacal light, starlight fainter than 6th K magnitude at dark sky (higher ecliptic and Galactic latitude), and thermal emission of the IPD at the ecliptic pole (Hauser et al. 1984). The NIRS has met its design objectives and will be able to make a highly sensitive spectral survey in the region which includes the window in the astrophysical foreground emission.

We are grateful to H. Okuda, H. Shibai, T. Onaka, and T. Watabe for help on this project and useful discussions. Thanks are also due to other members of the IRTS mission, including S. Sato, H. Matsuhara, and T. Hirao. This work was supported in part by the Daiko Science Foundation and the Scientific Research Fund of the Japanese Ministry of Education, Science, and Culture under grant 02952011.

REFERENCES

Berriman, G. B., Hauser, M. G., Boggess, N. W., Kelsall, T., Moseley, S. H., Silverberg, R. F., & Murdock, T. L. 1993, in AIP Conf. Proc. 278, Back to the Galaxy, ed. S. S. Holt & F. Verter (New York: AIP), 214
Carr, B. J., Bond, J. R., & Arnett, W. D. 1984, ApJ, 277, 445
Cowie, L. L., Gardner, J. P., Lilly, S. J., & McLean, I. 1990, ApJ, 360, L1
Giard, M., Pajot, F., Lamarre, J. M., Serra, G., Caux, E., Gispert, R., Leger, A., & Rouan, D. 1988, A&A, 201, L1
Gillett, F. C., Forrest, W. J., & Merrill, K. W. 1973, ApJ, 183, 87
Hauser, M. G. 1993, in AIP Conf. Proc. 278, Back to the Galaxy, ed. S. S. Holt & F. Verter (New York: AIP), 201
Hauser, M. G., et al. 1984, ApJ, 278, L15
Hauser, M. G., Kelsall, T., Moseley, S. H., Silverberg, R. F., Murdock, T., Toller, G., Spiesman, W., & Weiland, J. 1991, in AIP Conf. Proc. 222, After the First Three Minutes, ed. S. S. Holt, C. L. Bennett, & V. Trimble (New York: AIP), 161
Hayakawa, S., Matsumoto, T., Murakami, H., Uyama, K., Thomas, J. A., & Yamagami, T. 1981, A&A, 100, 116
Hofmann, W., & Lemke, D. 1978, A&A, 68, 389
Lamy, P. L., & Perrin, J. M. 1986, A&A, 163, 269
Lange, A. E., Freund, M., Sato, S., Hirao, T., Matsumoto, T., & Watabe, T. 1993, ApJ, 428, 384
Léger, A., & Puget, J. L. 1984, A&A, 137, L5
Leinert, C. 1975, Space Sci. Rev., 18, 281
Levasseur-Regourd, A. C., & Dumont, R. 1980, A&A, 84, 277
Matsumoto, T., Akiba, M., & Murakami, H. 1988, ApJ, 332, 575 (MAM)
Mattila, K. 1990, in IAU Symp. 139, Galactic and Extragalactic Background Radiation, ed. S. Bowyer & C. Leinert (Dordrecht: Kluwer), 257
McDowell, J. C. 1986, MNRAS, 223, 763
Murakami, H., Akiba, M., Matsumoto, T., & Noda, M. 1988, Japanese J. Appl. Phys., 27, L1973
Murakami, H., Noguchi, K., Matsumoto, T., Noda, M., Fujisada, H., Hara, K., & Sasase, T. 1987, in Infrared Astronomy with Arrays, ed. C. G. Wynn-Williams & E. E. Becklin (Honolulu: Univ. Hawaii), 41
Murakami, H., et al. 1994, ApJ, 428, 354
Natori, M., & Kuriki, K. 1991, Space Technol., 11, 159
Neugebauer, G., et al. 1984, ApJ, 278, L1
Noda, M. 1991, Ph.D. thesis, Nagoya Univ.
Noda, M., Christov, V. V., Matsuhara, H., Matsumoto, T., Matsuura, S., Noguchi, K., Sato, S., & Murakami, H. 1992, ApJ, 391, 456
Onaka, T., Yagi, T., Shibai, H., Murakami, H., Tanabe, T., & Kohno, T. 1994, Appl. Opt., in press
Partridge, R. B., & Peebles, P. J. E. 1967, ApJ, 148, 377
Roellig, T. L., Onaka, T., McMahon, T. J., & Tanabe, T. 1994, ApJ, 428, 370
Russell, R. W., Soifer, B. T., & Willner, S. P. 1977, ApJ, 217, L149
Sato, S., et al. 1994, in preparation
Shibai, H., Yui, M., Matsuhara, H., Hiromoto, N., Nakagaura, T., & Okuda, H. 1994, ApJ, 428, 377
Tyson, J. A. 1990, in IAU Symp. 139, Galactic and Extragalactic Background Radiation, ed. S. Bowyer & C. Leinert (Dordrecht: Kluwer), 245
Yamamoto, K., Fujisada, H., Matsumoto, T., & Murakami, H. 1989, Proc. SPIE, 1157, 338